Journal of New Approaches in Water Engineering and Environment
Online ISSN: 2981-0280
Homepage: https://nawee.gonbad.ac.ir

Combining pre-sedimentation with roughing filters: experimental evaluation of effective hydraulic parameters using a physical model

Behrouz Behzadfar[1], **HeydarAli Kashkuli**[1*], **Houshang Hasoonizadeh**[2], **Mohammad Heidarnejad**[1]

[1]Department of Water Science Engineering, khouzestan Science and Research Branch, Islamic Azad University, Ahvaz, Iran.
[2] Khuzestan Water and Power Organization, Ahvaz, Khuzestan, Iran.

Article Info

Article type:
Research Article

Article history:
Received 23 December 2025
Revised 17 February 2026
Accepted 05 August 2026
Published online 22 December 2026

Keywords:
Roughing filtration
Pre-sedimentation
High turbidity water
Physical modeling
Sustainable water treatment

ABSTRACT

Objective: Treatment of highly turbid surface water remains challenging in low-cost decentralized systems. This study aims to evaluate the hydraulic performance of a novel integrated pre-sedimentation and multilayer horizontal roughing filtration system and to develop dimensionless design relationships for improved process optimization and scale-up.

Methods: A laboratory-scale physical model was constructed in a hydraulic flume at the Khuzestan Water and Power Authority, Iran. The system combined a 1 m stilling basin with a three-layer roughing filter (20 mm, 10 mm, and 2 mm media). Experiments were conducted under three filter lengths (260, 350, and 450 cm), three filtration velocities (0.20, 0.60, and 1.00 m h^{-1}), three operation times (10, 20, and 30 min), and three influent turbidity ranges (1500–2500 NTU), resulting in 81 experimental runs. Turbidity removal efficiency was used as the performance criterion, and input predictability was assessed using the Gamma Test.

Results: Filter length was identified as the dominant parameter, improving removal efficiency by approximately 9–10% when increased from 260 to 450 cm. Maximum efficiencies exceeded 94% at 0.20 m h^{-1} and 450 cm length. Filtration velocity had a secondary negative effect (4–5% reduction across the tested range), while influent turbidity and operating time showed limited influence. The Gamma Test confirmed strong deterministic structure in the full-input configuration (Gamma = 0.0462; V-ratio = 0.1848).

Conclusions: The findings demonstrate that, within the tested range, increasing the effective length of the multilayer horizontal roughing filter improved turbidity removal performance and enhanced the overall efficiency of the combined pre-sedimentation–filtration system. These results indicate that filter length is an important design parameter for treating highly turbid surface waters in resource-limited regions. However, the present study should be interpreted as an experimental performance assessment of selected configurations rather than a formal geometric optimization, and determination of the absolute optimal design would require further investigation over a wider range of configurations together with techno-economic evaluation.

*Corresponding author, Email: kashkulihda@gmail.com

Cite this article: Behzadfar, B., Kashkuli, H.A., Hasoonizadeh, H. and Heidarnejad, M. (2026). Combining pre-sedimentation with roughing filters: experimental evaluation of effective hydraulic parameters using a physical model. *Journal of New Approaches in Water Engineering and Environment*, *5*(4), 65-89. https://doi.org/10.22034/nawee.2026.584356.1225

© The Author(s).
Publisher: Gonbad Kavous University.
DOI: https://doi.org/10.22034/nawee.2026.584356.1225

Introduction

In many fast-developing economies, the agricultural sector accounts for up to 90% of freshwater withdrawals, yet only 10% of generated wastewater undergoes adequate treatment. The discharge of untreated or partially treated wastewater introduces enteric pathogens and organic compounds into the environment, posing significant risks to irrigation and drinking water sources and underscoring the urgent need for simple, efficient treatment systems using locally available resources (Awandu et al., 2025; Nouri et al., 2025; Solgi et al., 2026). Addressing this challenge, particularly when dealing with extremely high-turbidity surface waters (1500–2500 NTU), is critical, as conventional systems often suffer from rapid clogging and high operational costs. This study evaluates an integrated treatment system consisting of pre-sedimentation and a multi-layer roughing filter. The primary objective is to analyze the impact of key design variables- namely filter length, filtration velocity, and filtration time- on turbidity removal efficiency, and to propose a physically based mathematical model to predict the system's performance. By employing this model and sensitivity analysis, the research aims to provide an optimal, robust design framework for effective water treatment in high-turbidity conditions (Fouad et al., 2016; Mao et al., 2021; Verma et al., 2017). Addressing this gap could substantially mitigate health risks in low-income regions through widespread implementation. Slow sand filtration (SSF) emerges as a promising solution, recognized for its cost-effectiveness and efficiency in reducing pathogens, particulate organic matter, and turbidity. Studies highlight its suitability as a tertiary treatment for municipal wastewater, achieving safe irrigation standards even at high hydraulic loading rates (HLR > 0.05 $m \cdot h^{-1}$). For instance, reductions of 1.95−2.46 log-units for fecal indicator bacteria (FIB) and 0.68–2.0 log-units for total coliforms have been documented, demonstrating SSF's robust performance. However, its application faces challenges in regions lacking locally available sand meeting specific grain size and uniformity coefficient requirements, emphasizing the need for adaptable material sourcing strategies to ensure broader accessibility (Jibhakate et al., 2017; Xie et al., 2022). To address these limitations and explore alternatives beyond conventional slow sand filtration, a range of studies has investigated diverse low-cost and adaptable treatment methods, as outlined in the following review.

Acharya and Parajuli (2026) investigated a dual-layer filter using crushed overburnt brick (COB) above sand to improve treatment of high-turbidity water (0–300 NTU). The optimal 30 cm COB + 30 cm sand configuration achieved 96.99% turbidity removal, kept effluent below 5.17 NTU, extended filter runs by 70%, and reduced backwash water by 39%. Awando et al. (2025) evaluated a horizontal roughing filter (HRF) using locally sourced gravel as a pretreatment unit for turbid surface water (300–450 NTU). Operating at 0.35–2.00 m/h, the system achieved an average turbidity removal of 93.68%, reducing turbidity to 8.8–25.02 NTU, meeting WHO requirements (<50 NTU) for subsequent slow sand filtration. Mtsweni et al. (2025) applied an artificial neural network (ANN) to predict clogging duration and effluent turbidity in horizontal roughing filters using inputs such as influent turbidity, filtration rate, pH, and conductivity. The optimized 4-8-2 ANN with the Levenberg–Marquardt algorithm

achieved MSE < 0.001 and R > 0.999, accurately predicting clogging and supporting proactive maintenance planning. Hamzani et al. (2025) investigated a combined synthetic filter and ultrafiltration (DHUSF-UF) system to treat highly turbid river water in Cempaka District. The system achieved turbidity removal efficiencies above 95% and consistently reduced turbidity to below 3 NTU, demonstrating its potential as an effective household- or community-scale water treatment solution. Aluah et al. (2025) evaluated a three-layer filter composed of chippings and river sand for treating wastewater sludge. The system achieved a 99.99% salinity reduction and decreased turbidity from 8198.67 to 19.0 NTU. The results demonstrated effective improvement of water quality, meeting standards for irrigation and non-critical reuse applications. Bachar et al. (2024) deployed biofilm-based slow sand filters in Tanzania, reducing turbidity from >10,000 to <5 NTU (meeting WHO standards) and lead (11 mg/L) via sedimentation and local materials (chalk/limestone). The low-tech system, enhanced by biofilm maturation, provided sustainable water purification for Maasai communities, demonstrating scalability in resource-limited settings. Tran et al. (2024) replaced rapid sand filters with ion exchange columns (polyacrylic A860 vs. polystyrene A502PS) for low-turbidity water. A860 (0.38 mm) caused higher head loss (151 cm vs. 101 cm) but better performance: turbidity 0.16–0.26 NTU (vs. 0.19–0.35 NTU) and DOC removal 25–37% (vs. 15–25%). NaCl (pH=12) partially restored A860 turbidity removal. Onyutha et al. (2024) optimized slow sand filters (SSF) with Ugandan natural/modified zeolite, achieving 75–98% lead (20–40 min), 91% As(III) (10 min), and 80% fluoride (5 min) removal. Optimal sand bed depths (453–580 mm) for turbidity (60–120 NTU) saved 35% sand costs, enhancing low-cost water treatment for high-turbidity, heavy metal-polluted sources. Fitriani et al. (2023) modified slow sand filters (SSF) with silica sand or Anadara granosa shells, achieving 82.07% turbidity, 89.5% total suspended solids (TSS), and 50.14% iron removal at 0.1 m/h. Optimal conditions prioritized higher flow rates (0.3 m/h, 68.4 L/day) for disaster areas, balancing efficiency and discharge needs using sand/geotextile/silica media. Moreira et al. (2023) tested coagulation-flocculation under high solids (2000–46,000 mg/L). FeCl3 yielded 201–26 NTU vs. organic coagulant (36–11 NTU), with >80% solids removal. Pre-thickeners (>20,000 mg/L) and ultrafiltration (130–136 L/m²h, <0.3 NTU) prevented sludge issues, ensuring plant operation under extreme turbidity. Fereidonian Dashti et al. (2018) optimized palm oil mill effluent (POME) treatment using calcined limestone filters via Response Surface Methodology. Under optimal conditions (800°C calcination, 20 mL/min flow, 4 mm media), turbidity removal reached 68%, outperforming raw limestone (55%). Adsorption isotherm data fit the Langmuir model (R^2=0.95). Freitas et al. (2021) tested compact (25 cm) vs. traditional (50 cm) household slow sand filters (HSSFs) over 436 days. Both achieved similar removals (turbidity: 13.2 ±14.6 NTU post-pretreatment; E. coli; p >0.05). Giardia cysts breached compact filters once; disinfection (NaOCl) inactivated bacteria, not protozoa. Compact HSSFs proved viable for decentralized use (48 L/day, 0.90 m³/m²/day). Kim et al. (2021) showed ZVI-sand filters (50% ZVI) reduced E. coli by >1.5 log CFU/mL in deionized water (98.8% efficiency) vs. pond water (63%) (p<0.001). Higher ZVI (50%) slightly outperformed 35% (p=0.48). Turbidity and conductivity impacted efficacy, with

lower turbidity enhancing removal. Zeng et al. (2018) evaluated pilot-scale up-flow roughing filters packed with ceramic media. The systems removed 60–90% of turbidity (1–500 NTU) and achieved ~70% NH_4^+-N reduction. Most solids accumulated within the lower 20 cm, contributing to head loss. Filter runs lasted 60–80 days, demonstrating suitability for rural water treatment applications. Duran Romero et al. (2020) found bio-sand filters (BSF) effectively treat water with turbidity (3-50 NTU), achieving 88–99% turbidity removal and log reductions of 0.54-2.01 (total coliform) and 1.2–2.2 (E. coli). Higher turbidity and 30-35 days' operation improved performance. Despite efficiency, additional disinfection is recommended for safe water. Nieto et al. (2020) developed a Gaussian process regression (GPR) model to predict sand filter outlet turbidity in microirrigation, analyzing 637 samples. Key variables (filter type, bed height, velocity, water quality) yielded a high-accuracy model (R^2=0.8921), enabling early turbidity detection to prevent emitter clogging in reclaimed effluent reuse. Babaei et al. (2019) achieved 98.22% COD, 99.97% LAS, 99.99% TSS, and 99.98% turbidity removal in greywater using a hybrid MSSF-MF-UF system. Effluent (0.04 mg/L LAS, 1.55 mg/L TSS, 1.04 NTU) met reuse standards despite higher OLRs reducing efficiency. Biofilm-enhanced MSSF and membrane synergy ensured effective LAS/SS removal. Varma et al. (2017) emphasized slow sand filtration (SSF) (0.1–0.2 m^3/h flow rate) as a low-cost, understudied method, effectively removing pathogens (E. coli, Giardia), turbidity, and metals to meet potable/non-potable standards. Napotnik et al. (2017) found bucket-sized biosand filters (2-5 gal) matched traditional concrete filters over 9 months, achieving <0.6 NTU turbidity and 72-78% of samples with <1 CFU/100mL. Smaller sand beds didn't affect performance, but frequent refilling's impact on pause periods needs study for scaled-down BSFs. Khan and Farooqi (2011) investigated up-flow roughing filtration as a pre-treatment for high-turbidity water in the Chakwal Water Treatment Plant. The system reduced turbidity by over 90%, decreased coagulant dosage and sludge production, extended filter runs, and was estimated to save more than US $54,000 annually in coagulant costs. El-Taweel and Ali (2000) evaluated roughing filter media made from locally available materials for removing turbidity and organic matter from surface water. A three-layer gravel filter achieved 84–100% microbial removal and 83% turbidity reduction, which increased to 92% when followed by slow sand filtration.

Despite the significant body of research on roughing filtration and its variants, several critical gaps remain in understanding integrated treatment systems. Most existing studies have focused on the performance of isolated, single-stage units (e.g., standalone horizontal or dynamic roughing filters, or pretreatment before slow sand filtration), often overlooking the synergistic benefits of an optimized pre-sedimentation stage specifically integrated with multilayer roughing media. Furthermore, the investigated operating durations (10–30 min) represent short-term filtration behavior and do not capture long-term operational processes such as progressive clogging, head-loss accumulation, media fouling, and potential filter aging effects that may influence system performance over extended periods. Specifically, the derivation of scalable, dimensionless relationships-essential for engineering design and system optimization in varying field conditions- has not been adequately addressed in the context of

locally sourced, multilayer media configurations. Consequently, the precise interaction between retention time, filter length, and grading pattern governing overall efficiency in these combined systems remains insufficiently quantified. Accordingly, the present study addresses this gap by experimentally evaluating a combined pre-sedimentation–multilayer roughing filtration system with locally available media and by developing dimensionless relationships for design and scale-up purposes. This integrated and design-oriented approach represents the main novelty of the study compared with previous, more compartmentalized, roughing filter investigations.

Based on the identified research gaps, this study aims to investigate the hydraulic and operational performance of an integrated pre-sedimentation–multilayer roughing filtration system for the treatment of high-turbidity water. The study is guided by the following research questions: (1) How do key hydraulic parameters, including filtration velocity and retention time, influence turbidity removal efficiency in the combined system? (2) How do geometric characteristics such as filter length and media gradation affect the overall filtration performance? (3) Can dimensionless relationships be developed to describe the interaction between hydraulic and geometric parameters for design and scale-up purposes? It is hypothesized that integrating pre-sedimentation with multilayer roughing filtration significantly improves turbidity removal under high-turbidity conditions and that the interaction between hydraulic and geometric parameters can be represented through predictive dimensionless relationships applicable for engineering design.

1. Materials and Method

1.1 Experimental setup

The experimental program was designed to evaluate the performance of a combined pre-sedimentation and multilayer horizontal roughing filtration system for the treatment of highly turbid surface water under controlled laboratory conditions. All experiments were conducted in the hydraulic flume of the Khuzestan Water and Power Authority, Iran. The flume was 6.0 m long, 1.5 m wide, and 1.5 m high (Fig. 1), providing sufficient length to accommodate both the pre-sedimentation zone and the filtration units while maintaining stable hydraulic conditions. The flume therefore served as a controlled laboratory-scale physical model for investigating the hydraulic and filtration behavior of the combined pre-sedimentation–roughing filtration system.

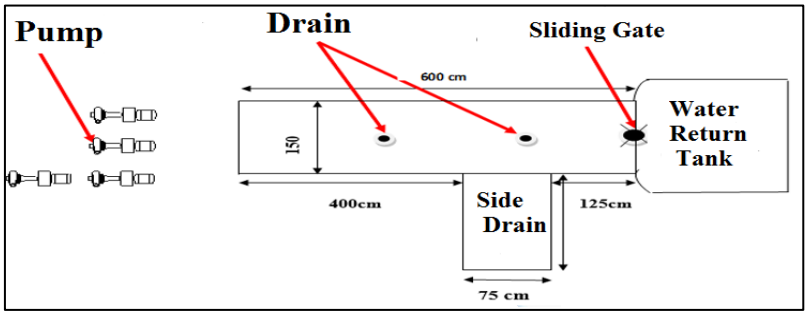

Figure 1- A schematic view of experimental installation

Highly turbid influent water was prepared in a recirculation tank located downstream of the flume by manually adding fine sediment and continuously mixing until the desired turbidity levels were achieved. Three representative turbidity ranges were selected- 1500-1600 NTU, 1900–2000 NTU, and 2400–2500 NTU- to simulate extreme sediment loads commonly observed in regional rivers during flood events. Prior to filtration, the prepared water entered a 1 m stilling basin located at the upstream end of the flume, which served as a pre-sedimentation zone to dampen flow turbulence and promote partial settling of coarse suspended particles. Downstream of the stilling basin, water flowed horizontally through a multilayer roughing filter composed of three granular media layers arranged sequentially from coarse to fine. Basic water quality conditions were monitored during the experiments to ensure stable influent characteristics. The influent water exhibited near-neutral pH conditions and moderate electrical conductivity typical of laboratory tap water. The experiments were conducted under stable laboratory conditions, and water temperature remained within the typical indoor range of approximately 20–25 °C throughout all test runs. No intentional heating or cooling was applied, and temperature fluctuations were minimal during the short-duration experiments. No chemical coagulants or additives were used, and the removal of turbidity was achieved solely through physical filtration processes within the roughing filter system. The filter bed was composed of three granular layers: coarse gravel (nominal size ≈20 mm), medium gravel (≈10 mm), and fine sand with an average grain diameter of approximately 2 mm. This graded configuration was designed to promote progressive particle removal and hydraulic stability within the filtration system. Although detailed sieve analysis parameters (e.g., D_{10}, D_{50}, Cu) were not determined, the nominal size classification provided by the supplier was used to ensure consistent grading across experimental runs. In the reference configuration, the respective layer lengths were 2.50 m, 1.25 m, and 0.75 m, yielding a total filter length of 5.50 m. All layers had a uniform depth of 0.80 m and extended across the full width of the flume (Fig. 2). To investigate the influence of filter geometry, three different effective filter lengths- 260, 350, and 450 cm- were examined by proportionally modifying the longitudinal extent of the media layers while preserving their gradation order and depth. Each experimental condition was conducted in triplicate to ensure experimental reliability and reproducibility. The reported results correspond to the average values of the repeated runs, and the observed variations between replicates were minimal. These configurations are summarized in Table 1. In this table, column (1) represents turbidity, column (2) represents the filtration velocity, column (3) represents time, column (4) represents the sand filter length, and column (5) represents efficiency.

Figure 2- Filter layout in the laboratory flume

Table 1- Included data of the present work

No.	(1)	(2)	(3)	(4)	(5)	No.	(1)	(2)	(3)	(4)	(5)
1	1510	0.2	10	450	94.97	42	1964	0.6	20	260	81.16
2	1504	0.2	10	350	95.01	43	1925	0.6	30	450	95.22
3	1550	0.2	10	260	94.19	44	1932	0.6	30	350	91.12
4	1503	0.2	20	450	94.94	45	1966	0.6	30	260	80.12
5	1520	0.2	20	350	95.07	46	1950	1.0	10	450	94.36
6	1551	0.2	20	260	93.87	47	1934	1.0	10	350	90.02
7	1550	0.2	30	450	94.97	48	1919	1.0	10	260	81.97
8	1520	0.2	30	350	94.8	49	1980	1.0	20	450	94.10
9	1504	0.2	30	260	93.48	50	1934	1.0	20	350	89.09
10	1520	0.6	10	450	89.35	51	1932	1.0	20	260	81.39
11	1506	0.6	10	350	91.14	52	1900	1.0	30	450	94.23
12	1510	0.6	10	260	89.93	53	1950	1.0	30	350	91.82
13	1510	0.6	20	450	89.11	54	1911	1.0	30	260	80.46
14	1550	0.6	20	350	89.66	55	2420	0.2	10	450	95.16
15	1535	0.6	20	260	90.25	56	2425	0.2	10	350	90.23
16	1501	0.6	30	450	91.14	57	2444	0.2	10	260	80.19
17	1550	0.6	30	350	90.32	58	2425	0.2	20	450	95.89
18	1541	0.6	30	260	90.32	59	2430	0.2	20	350	89.34
19	1506	1.0	10	450	82.24	60	2436	0.2	20	260	80.33
20	1503	1.0	10	350	82.10	61	2420	0.2	30	450	94.30
21	1570	1.0	10	260	82.69	62	2421	0.2	30	350	89.10
22	1550	1.0	20	450	82.34	63	2416	0.2	30	260	80.19
23	1503	1.0	20	350	81.39	64	2450	0.6	10	450	94.44
24	1541	1.0	20	260	82.38	65	2435	0.6	10	350	89.15
25	1510	1.0	30	450	82.16	66	2416	0.6	10	260	80.96
26	1503	1.0	30	350	81.40	67	2452	0.6	20	450	94.53
27	1519	1.0	30	260	82.10	68	2485	0.6	20	350	91.12
28	1910	0.2	10	450	94.11	69	2430	0.6	20	260	80.93
29	1911	0.2	10	350	90.29	70	2456	0.6	30	450	95.29
30	1919	0.2	10	260	82.15	71	2490	0.6	30	350	90.39
31	1980	0.2	20	450	94.85	72	2436	0.6	30	260	80.37
32	1920	0.2	20	350	90.46	73	2452	1.0	10	450	95.60
33	1932	0.2	20	260	82.73	74	2490	1.0	10	350	97.87
34	1910	0.2	30	450	94.32	75	2490	1.0	10	260	80.47
35	1970	0.2	30	350	90.33	76	2490	1.0	20	450	95.19
36	1970	0.2	30	260	80.33	77	2411	1.0	20	350	89.40
37	1912	0.6	10	450	95.62	78	2497	1.0	20	260	80.52
38	1975	0.6	10	350	90.00	79	2489	1.0	30	450	95.86
39	1965	0.6	10	260	81.73	80	2425	1.0	30	350	89.55
40	1925	0.6	20	450	95.39	81	2411	1.0	30	260	81.87
41	1935	0.6	20	350	91.25						

Figure 3- Filter layout in the laboratory flume

Filtration experiments were performed at three superficial filtration velocities of 0.20, 0.60, and 1.00 m h^{-1}, corresponding to progressively increasing hydraulic loading conditions. Flow rates were regulated using a calibrated rotameter (Fig. 3a), and downstream water levels were controlled via an adjustable slide gate to prevent filter submergence.

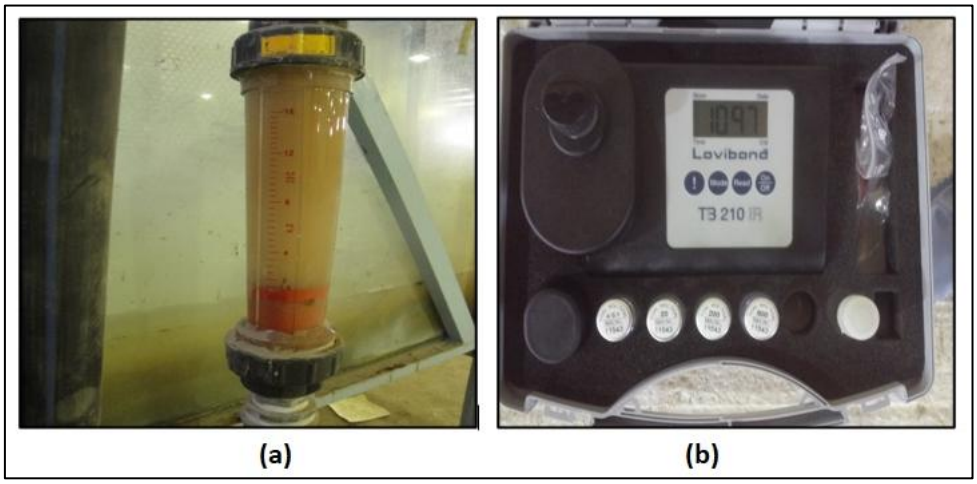

Figure 4- (a) Turbidimeter; (b) Rotameter

For each combination of influent turbidity, filtration velocity, and filter length, experiments were conducted for operation times of 10, 20, and 30 min. Influent turbidity was measured directly in the return tank using a Lovibond TS 210 turbidimeter (Fig. 3b), while effluent turbidity was recorded immediately downstream of the third filter layer to capture the cumulative filtration performance. A total of 81 experimental runs were carried out, covering all combinations of the investigated parameters. Filtration performance was quantified using turbidity removal efficiency, defined as:

(1)

2. Results and discussion

2.1 Experimental outcomes

Fig. 4 illustrates the influence of filter length on turbidity removal efficiency at three filtration velocities of 0.20, 0.60, and 1.00 $m \cdot h^{-1}$, with efficiency values averaged over all influent turbidity levels and operation times. A clear and monotonic increase in filtration efficiency is observed with increasing filter length for all hydraulic loading conditions, confirming the dominant role of geometric extension in enhancing particle removal.

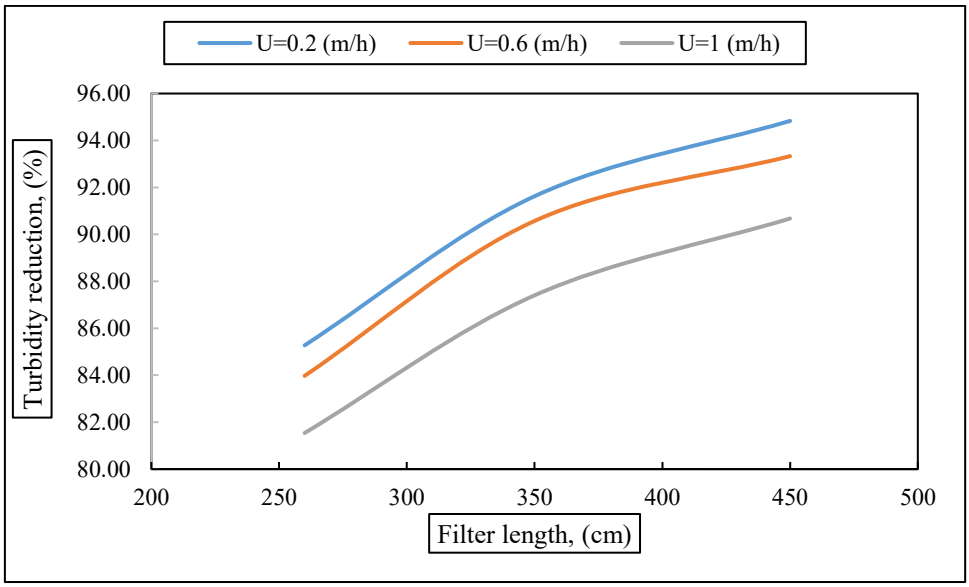

Figure 5- Effects of filter length on efficiency

At the lowest filtration velocity of 0.20 $m \cdot h^{-1}$, increasing the filter length from 260 to 450 cm results in an increase in mean turbidity removal efficiency from approximately 85.3 % to 94.8 %, corresponding to an absolute gain of nearly 9.5 percentage points. A similar trend is observed at a filtration velocity of 0.60 $m \cdot h^{-1}$, where efficiency increases from about 84.0 % at 260 cm to 93.3 % at 450 cm, yielding an improvement of approximately 9.3 %. Even under the highest hydraulic loading (1.00 $m \cdot h^{-1}$), extending the filter length produces a substantial performance enhancement, with mean efficiency rising from 81.5 % to 90.7 %, corresponding to an increase of 9.2 %. The nearly parallel slopes of the three curves indicate that the positive effect of filter length is largely independent of filtration velocity within the investigated range. This suggests that increasing filter length consistently enhances hydraulic residence time and available surface area for sediment interception, sedimentation, and attachment, regardless of flow regime. In contrast, the vertical separation between the curves reflects the secondary influence of filtration velocity, which primarily modulates efficiency within a narrower band of approximately 3-5 % for a given filter length. In addition, the purpose of presenting Figure 4 was not merely to confirm the positive effect of length, but to quantify the rate of improvement in removal efficiency under different hydraulic conditions and to support the development of scalable experimental relationships. From a practical design perspective, however, the

hydraulic advantage of increasing filter length should be interpreted together with engineering constraints such as construction cost, land requirement, and operational feasibility. Although increasing filter length resulted in higher turbidity removal efficiency, this improvement should be interpreted together with practical design constraints. In real-world applications, longer filters require more construction material, greater land area, and potentially higher installation and maintenance efforts. The present study was focused on the hydraulic and treatment performance of the system under controlled laboratory conditions; therefore, a detailed economic analysis was not included. Accordingly, the superiority of longer filter lengths in this study refers only to treatment performance within the investigated range and should not be interpreted as a universal economic recommendation. Fig. 4 shows that increasing the filter length from 260 to 450 cm improved turbidity removal efficiency by about 9-10%, indicating that filter length was the most influential design parameter within the tested range. This result highlights the importance of filter length in the performance of multilayer roughing filters for highly turbid waters, without implying a formal geometric optimization of the system.

Fig. 5 presents the effect of filtration velocity on turbidity removal efficiency for three filter lengths (260, 350, and 450 cm), with efficiency values averaged over all influent turbidity levels and operational times. In contrast to filter length, filtration velocity exhibits a consistent but comparatively moderate negative influence on treatment performance across all filter configurations.

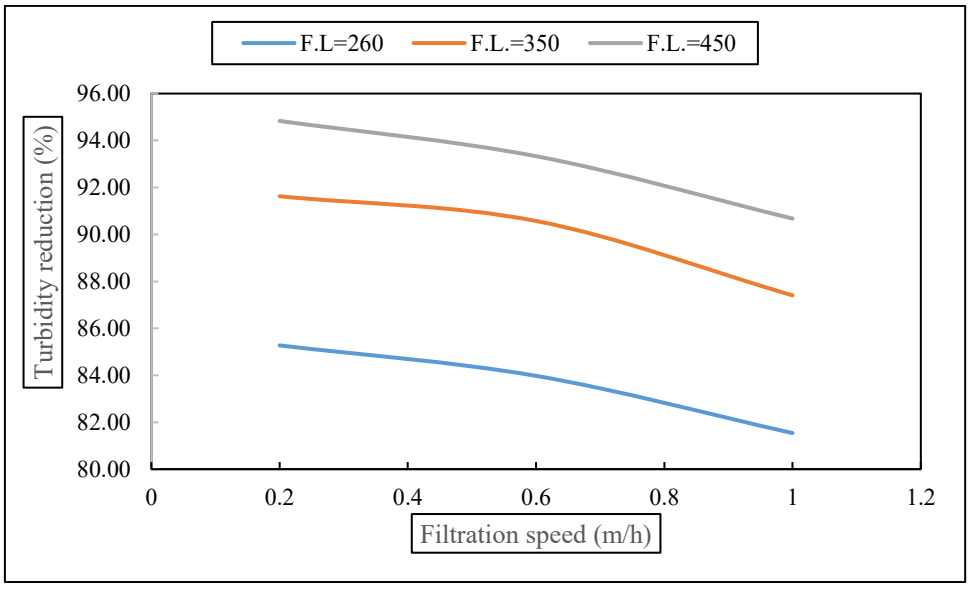

Figure 6- Effects of filtration velocity on efficiency

For the shortest filter length (260 cm), increasing the filtration velocity from 0.20 to 1.00 m·h^{-1} results in a reduction in mean turbidity removal efficiency from approximately 85.3 % to 81.5 %, corresponding to an absolute decrease of about 3.8 percentage points. A similar trend is observed for the intermediate filter length of 350 cm, where efficiency declines from around 91.6 % at 0.20 m·h^{-1} to 87.4 % at 1.00 m·h^{-1}, yielding a reduction of approximately 4.2 %. For the longest filter length (450 cm), efficiency decreases from about 94.8 % to 90.7 %

over the same velocity range, corresponding to a decline of roughly 4.1 %. The nearly parallel slopes of the three curves indicate that the adverse effect of increasing filtration velocity is relatively uniform across different filter lengths. This behavior suggests that higher hydraulic loading primarily reduces contact time and limits particle deposition efficiency, rather than altering the fundamental removal mechanisms within the filter bed. Notably, even at the highest filtration velocity of 1.00 $m \cdot h^{-1}$, turbidity removal efficiency remains above 90 % for the 450 cm filter, demonstrating that sufficient filter length can effectively compensate for increased flow velocity. Fig. 5 confirms that filtration velocity was a secondary control parameter compared with filter length. Increasing velocity from 0.20 to 1.00 $m \cdot h^{-1}$ reduced efficiency by about 4-5%, which was notably smaller than the 9-10% gain achieved by increasing filter length from 260 to 450 cm. These results highlight the importance of filter length in maintaining high treatment efficiency under variable hydraulic loading conditions.

Table 2 presents a heatmap summarizing the combined effects of filter length and filtration velocity on turbidity removal efficiency. The reported values represent mean efficiencies averaged over all influent turbidity levels and operational times, allowing direct comparison of the relative influence of geometric and hydraulic parameters. The results clearly indicate that filter length is the dominant factor controlling turbidity removal efficiency. At a constant filtration velocity of 0.20 $m \cdot h^{-1}$, increasing the filter length from 260 to 350 cm improves the average efficiency from 85.27 % to 91.63 %, corresponding to an increase of 6.36 percentage points. Further extension of the filter length to 450 cm results in an efficiency of 94.83 %, yielding an overall improvement of approximately 9.6 % compared to the shortest filter. A similar pattern is observed at higher filtration velocities. At 0.60 $m \cdot h^{-1}$, mean turbidity removal increases from 83.97 % (260 cm) to 90.57 % (350 cm) and reaches 93.33 % at a filter length of 450 cm. Likewise, at the highest velocity of 1.00 $m \cdot h^{-1}$, extending the filter length enhances efficiency from 81.54 % to 87.40 % and 90.68 %, resulting in a total gain of approximately 9.1 percentage points. In contrast, the effect of filtration velocity at a fixed filter length is comparatively moderate. For a filter length of 260 cm, increasing velocity from 0.20 to 1.00 $m \cdot h^{-1}$ reduces efficiency by 3.73 %. Corresponding reductions of 4.23 % and 4.15 % are observed for filter lengths of 350 and 450 cm, respectively. This indicates that while higher velocities slightly diminish turbidity removal due to reduced contact time, their impact remains secondary compared to geometric extension of the filter bed. Overall, the heatmap demonstrates a steeper efficiency gradient along the filter length axis than along the filtration velocity axis, confirming that increasing filter length provides a more effective and robust strategy for enhancing turbidity removal performance. The highest efficiencies (> 94 %) are achieved at a filter length of 450 cm and a filtration velocity of 0.20 $m \cdot h^{-1}$, whereas the lowest efficiencies (≈ 81–83 %) occur at the shortest filter length combined with the highest velocity.

Table 2- Heatmap of turbidity reduction

		Filtration velocity (m/h)		
		0.2	**0.6**	**1**
Filter length (cm)	**260**	85.27	83.97	81.54
	350	91.63	90.57	87.40
	450	94.83	93.33	90.68

Fig. 6 illustrates the effect of influent turbidity on filtration efficiency using box-and-whisker plots for three turbidity ranges (1500–1600, 1900–2000, and 2400–2500 NTU). The distributions summarize efficiency values obtained under all combinations of filter length, filtration velocity, and operation time, thereby highlighting the isolated influence of influent turbidity. The results indicate that influent turbidity has a negligible effect on turbidity removal efficiency within the investigated range. The median efficiencies for the three turbidity classes remain remarkably close, lying at approximately 90.1 %, 90.3 %, and 90.4 %, respectively. Similarly, the mean efficiencies show minimal variation and remain confined to a narrow interval of less than 0.5 percentage points, confirming the absence of a systematic trend with increasing influent turbidity. The interquartile ranges (25–75 %) for all three turbidity levels are also comparable, spanning roughly from 82 % to 94 %, indicating similar variability patterns regardless of influent turbidity. Moreover, the overall efficiency ranges (including whiskers and outliers) largely overlap, further demonstrating that changes in influent turbidity from 1500 to 2500 NTU do not significantly alter filtration performance. No consistent shift in either dispersion or central tendency is observed across the turbidity classes. These findings suggest that, within the studied turbidity interval, the filtration system operates under a removal regime that is primarily governed by filter geometry and hydraulic loading, rather than by influent turbidity itself. The weak sensitivity to influent turbidity may be attributed to the dominance of physical straining and sedimentation mechanisms within the filter bed, which remain effective even at high particulate concentrations. Therefore, Fig. 6 confirms that influent turbidity acts as a secondary or negligible parameter in determining turbidity removal efficiency compared to filter length and filtration velocity. This observation supports the robustness of the filtration system for treating highly turbid waters without requiring operational adjustment across the examined turbidity range.

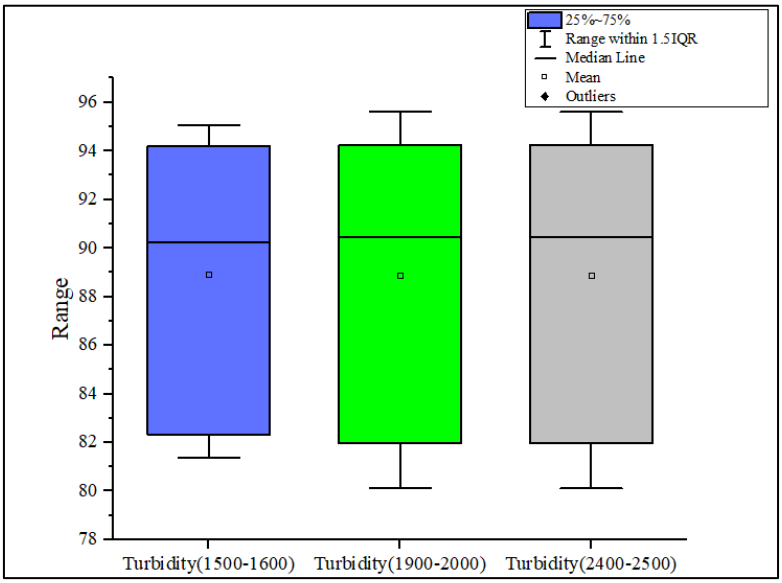

Figure 7-Effect of influent turbidity on filtration efficiency

Fig. 7 presents the influence of filtration time on turbidity removal efficiency using box-and-whisker plots for three operational durations (10, 20, and 30 min). The efficiency distributions are compiled from all combinations of influent turbidity, filter length, and filtration velocity, enabling an isolated evaluation of the effect of time. The results show that filtration time has a minimal influence on removal efficiency within the investigated range. Median efficiencies for filtration times of 10, 20, and 30 min are approximately 90.2 %, 89.8 %, and 90.4 %, respectively, indicating no monotonic or systematic trend with increasing time. The mean efficiencies similarly remain confined to a narrow interval of less than 0.6 percentage points, confirming the weak sensitivity of efficiency to operational duration. The interquartile ranges (25–75 %) for all three time intervals are nearly identical, extending roughly from 82 % to 94 %, which suggests comparable variability regardless of filtration time. Furthermore, the overall efficiency ranges (including whiskers and outliers) substantially overlap, demonstrating that extending filtration time from 10 to 30 minutes does not lead to a significant improvement in turbidity removal performance. These observations imply that the majority of turbidity removal occurs during the early stages of filtration, and that prolonging the filtration time beyond 10 minutes yields diminishing returns under the tested conditions. This behavior is consistent with filtration mechanisms dominated by rapid physical straining and initial particle capture within the filter bed. Fig. 7 confirms that filtration time is a secondary parameter compared to filter length and filtration velocity. Adjusting filtration duration within the range of 10–30 minutes does not substantially affect efficiency, highlighting that system performance is primarily governed by geometric and hydraulic characteristics rather than operational time.

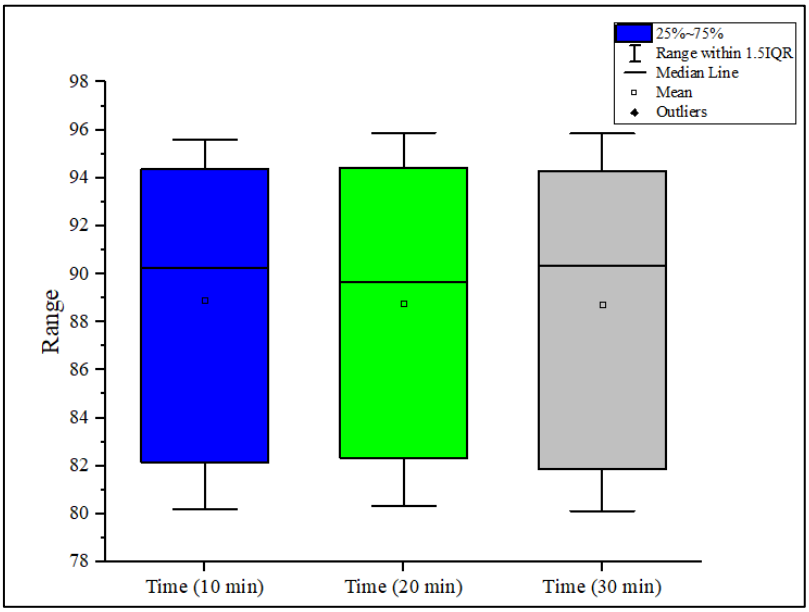

Figure 8- Effect of time on filtration efficiency

Recent studies on roughing filtration systems have similarly reported that filter length plays a critical role in improving turbidity removal efficiency. For example, several investigations have shown that longer filter beds provide greater particle deposition and longer contact time between suspended solids and the filter media, resulting in higher removal efficiencies. The present findings are consistent with these observations, as increasing the filter length from 260 to 450 cm significantly enhanced turbidity removal performance. In addition, previous studies have indicated that higher filtration velocities tend to reduce removal efficiency due to reduced particle settling and attachment within the filter media. A similar trend was observed in the current study, where increasing filtration velocity from 0.20 to 1.00 m h^{-1} caused a moderate decrease in treatment efficiency. However, the integrated configuration used in this study, which combines pre-sedimentation with multilayer roughing filtration, demonstrated stable performance even under very high influent turbidity levels (up to 2500 NTU), highlighting the potential applicability of this approach for highly sediment-laden surface waters.

Although the general trends observed in this study are consistent with previous roughing filtration research, the absolute turbidity removal efficiencies differ from some values reported in the literature. These differences can be attributed to several factors. First, the present system incorporates a pre-sedimentation zone upstream of the multilayer roughing filter, which likely reduced the incoming particulate load and improved the overall removal efficiency compared with single-stage filtration systems. Second, the experiments were conducted under very high influent turbidity conditions, which may alter particle–media interactions and deposition behavior relative to studies performed at lower turbidity levels. Third, variations in filter media size, gradation, bed structure, and effective filter length can significantly affect particle capture mechanisms. In addition, differences in filtration velocity, operating time, sediment characteristics, and laboratory versus field-scale conditions may further contribute to discrepancies between studies. Therefore, direct comparison of absolute efficiency values

should be made with caution, and the present results should be interpreted within the specific hydraulic and structural conditions of the tested system.

2.2 Mathematical modeling

2.2.1 Sensitivity analysis

The Gamma Test was used as a model-independent sensitivity analysis approach to identify the optimal combination of operational parameters affecting filtration efficiency, including initial turbidity, filtration velocity, filtration time, and filter length. The system response is assumed to follow (Shakeri yousefi et al., 2025):

(2)

where y denotes filtration efficiency, x is the vector of input parameters, f(x) is an unknown smooth function, and ε represents random noise. For each observation, the squared Euclidean distance to its k-th nearest neighbor in the input space and the corresponding output difference are computed as

(3)

(4)

A linear regression is then established:

(5)

where the intercept provides an estimate of the minimum achievable mean squared error, i.e.,

(6)

To normalize this measure, the V-ratio is defined as

(7)

Lower values of and V-ratio indicate stronger input–output dependency and higher predictability. Accordingly, the optimal filtration parameter combination was determined as the one yielding the minimum and V-ratio values. The -test results (Table 3) indicate that increasing the number of input parameters significantly improves model predictability, as reflected by lower Gamma and V-ratio values. The full-input configuration (Mask=1111) achieved the minimum Gamma (0.0462) and V-ratio (0.1848), demonstrating the strongest deterministic structure and the lowest unexplained variance. In contrast, reduced or single-parameter masks exhibited substantially higher V-ratio values (up to 1.1595), confirming weaker input–output relationships and diminished filtration performance sensitivity.

Table 3- Criteria for selecting the best combination of independent variables

Gamma	Gradient	Standard	V-Ratio	Mask
0.0462	0.1592	0.0559	0.1848	1111
0.0504	0.2136	0.0708	0.2017	1101
0.0469	0.1295	0.0706	0.1874	0110
0.0722	0.5289	0.0266	0.2888	1001
0.1396	0.0709	0.0549	0.5583	0111
0.1531	-0.0055	0.0573	0.6125	1011
0.2512	-0.1171	0.0209	1.0049	1110
0.1346	0.0999	0.06	0.5383	0101
0.168	0.0627	0.0702	0.6721	0011
0.2013	0.0959	0.0473	0.8052	1100
0.2532	-0.7347	0.0286	1.0128	1000
0.2729	-0.1219	0.0275	1.0914	1010
0.1835	0.1637	0	0.734	0001
0.2899	-0.1231	0	1.1595	0010
0.2484	-0.0451	0	0.9936	0100

Based on the experimental observations and the sensitivity analysis conducted using the Gamma test, the filtration system investigated in this study exhibits a pronounced deterministic structure, particularly when geometric, hydraulic, and temporal parameters are jointly considered. The minimum Gamma (0.0462) and V-ratio (0.1848) obtained for the full-input configuration (Mask = 1111) indicate that turbidity removal efficiency can be represented by a smooth nonlinear function of filter length, filtration velocity, influent conditions, and operational time, with a relatively low level of unexplained variance. Experimental results clearly demonstrated that filter length is the dominant parameter governing turbidity removal efficiency, whereas filtration velocity plays a secondary but systematic role. In contrast, filtration time showed a weak marginal influence within the investigated range (10–30 min), as confirmed by the overlapping distributions in Figure 7. This behavior suggests that the majority of particle removal occurs during the early stages of filtration, followed by a gradual transition toward a quasi-steady or saturated state. Such a response is characteristic of filtration mechanisms dominated by rapid physical straining and initial particle capture within the filter bed. Accordingly, the functional form of the predictive model must satisfy three essential physical requirements:

(i) An asymptotic increase in efficiency toward a maximum attainable value,

(ii) A strong dependence on hydraulic residence time controlled primarily by filter length and flow velocity, and

(iii) a diminishing contribution of filtration time reflecting early-stage dominance and subsequent saturation.

To meet these requirements, turbidity removal efficiency η is assumed to follow a nonlinear saturation-type behavior and may be expressed in the general form:

(8)

where represents the maximum achievable removal efficiency under ideal conditions, and and are a dimensionless performance function incorporating geometric, hydraulic, and temporal effects. From a physical perspective, the ratio represents an effective hydraulic residence time within the filter media and therefore governs the opportunity for particle interception, sedimentation, and attachment. To incorporate the observed diminishing influence of operational time, a bounded exponential term is introduced to describe the rapid initial removal followed by saturation. Consequently, the performance function may be formulated as:

(9)

(10)

where k is a system-specific filtration efficiency coefficient reflecting media characteristics and capture potential, α is a time-attenuation parameter controlling the rate at which filtration efficiency approaches its asymptotic state, Tu_{ref} is initial turbidity. Substituting this expression into the governing equation yields the proposed nonlinear semi-empirical model:

(11)

This formulation is fully consistent with the experimental findings and the Gamma-test-based sensitivity analysis. In particular, the model explicitly preserves the dominant role of filter length, accounts for the secondary influence of filtration velocity through hydraulic residence time, and incorporates filtration time in a physically meaningful manner that reflects its diminishing marginal effect. The parameters , k, Tu_{ref}, α and β can be estimated through nonlinear regression using the experimental dataset, enabling quantitative prediction of turbidity removal efficiency across a wide range of operating conditions.

(12)

The proposed physically-based model was calibrated using nonlinear least squares applied to the complete experimental dataset (81 runs). The maximum achievable turbidity removal efficiency was estimated as , representing the saturation limit of the combined pre-sedimentation and roughing filtration system. The geometric–hydraulic coefficient k=0.00864 confirms the dominant influence of the length-to-velocity ratio , in agreement with the experimental sensitivity analysis. The temporal coefficient α=3.09 min^{-1} indicates rapid attainment of steady-state performance, explaining the limited effect of operational time beyond the initial minutes. A weak corrective exponent β=0.00221 was introduced to account for variations in influent turbidity, improving predictive accuracy without compromising physical interpretability.

Table 4 presents the statistical performance indicators for the developed predictor (Eq. 12) during both the training and testing phases. The metrics, including root mean square error (RMSE), coefficient of determination (R^2), mean absolute error (MAE), and Nash–Sutcliffe

efficiency (NSE), were employed to assess the model's accuracy. The results indicate that the empirical model captures the overall trend of the filtration process with a consistent performance across both datasets. The model yielded an R^2 of 0.2935 and 0.2702, and an NSE of 0.2916 and 0.2657 for the training and testing phases, respectively. The consistency between training and testing metrics confirms that the model is not overfitted and maintains stability when applied to unseen data. While the absolute performance metrics are moderate, they reflect the inherent stochastic nature of the roughing filtration process and the influence of complex, non-linear variables that are often difficult to fully capture with empirical predictors.

Table 4- Performance metrics of developed predictor (Eq. 12)

	RMSE	R^2	MAE	NSE
Training phase	4.6440	0.2935	3.6713	0.2916
Testing phase	5.1043	0.2702	4.1365	0.2657

Fig. 9 displays the probability density distributions of the measured and predicted removal efficiencies across both the training (left) and testing (right) phases. During the training phase, which was utilized to calibrate the model parameters and extract the empirical equation, the model successfully captures the central tendency of the experimental data, smoothing out the multimodal fluctuations of the physical runs into a stable, unimodal prediction centered around 90%. More importantly, in the testing phase (right)- where the calibrated empirical equation was independently evaluated against unseen test data- the prediction profile remains highly consistent with the training phase. The close agreement between the training and testing density distributions proves that the empirical model is mathematically robust, generalizes well to new operational scenarios, and does not suffer from overfitting.

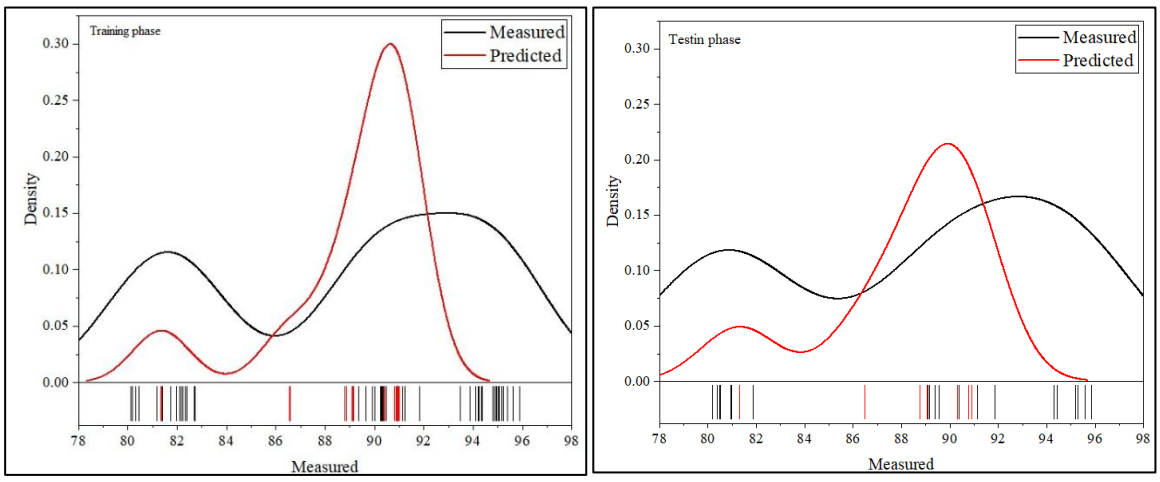

Figure 9- Density distribution of measured vs. predicted values of η

To further evaluate the local concentration and agreement between the experimental and predicted results, a two-dimensional kernel density analysis was performed for both the training and testing datasets (Fig. 10). The contour plots illustrate the localized density of data points, where the red hotspots indicate the regions with the highest frequency of observations. In the training phase (left), the highest density of points is concentrated at high removal efficiencies,

specifically around the coordinates where both measured and predicted values lie between 90% and 92%. A similar high-density hotspot is observed in the independent testing phase (right) within the 90–95% efficiency range. This alignment of high-density zones between the calibration (training) and validation (testing) phases confirms that the empirical model consistently replicates the most critical operating regions of the roughing filter without systematic bias, demonstrating its reliability for practical design applications.

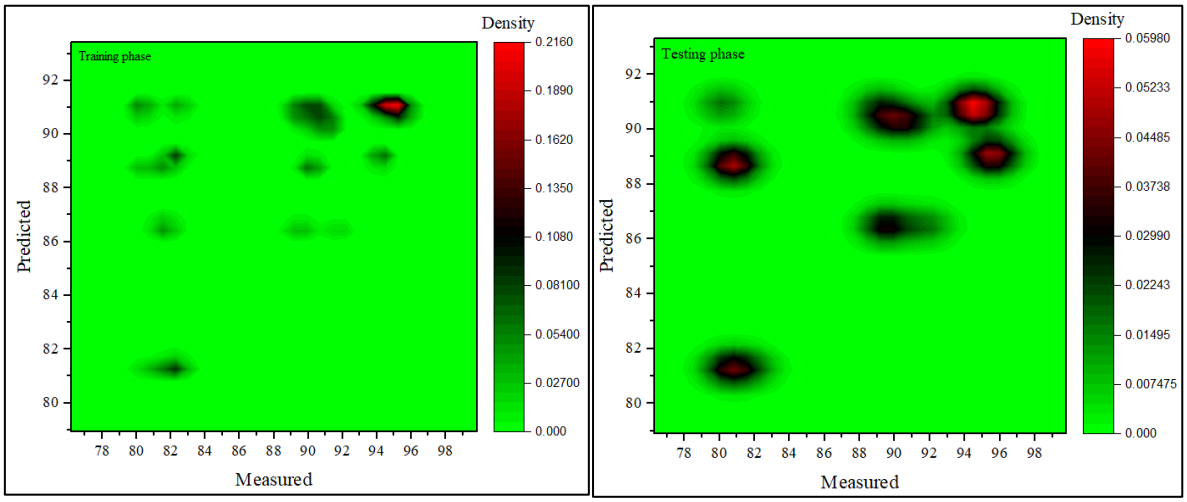

Figure 10- 2D kernel density plots of measured vs. predicted η

Fig. 11 presents a boxplot comparison of the measured and predicted removal efficiencies during the training and testing phases to evaluate the distribution characteristics and spread of the data. For both phases, the median values (indicated by the horizontal lines inside the boxes) of the predicted efficiencies closely align with those of the measured datasets, centering near 90%. However, the measured data exhibits a wider interquartile range (IQR) and overall spread, capturing the natural fluctuations and experimental variability inherent in the physical system. In contrast, the predicted boxplot is more compact, reflecting the model's tendency to predict the central operational trend. Crucially, the consistency in box structures, medians, and data ranges between the training (left) and independent testing (right) phases demonstrates that the empirical model maintains its predictive accuracy and structural stability when applied to unseen validation data, showing no signs of overfitting.

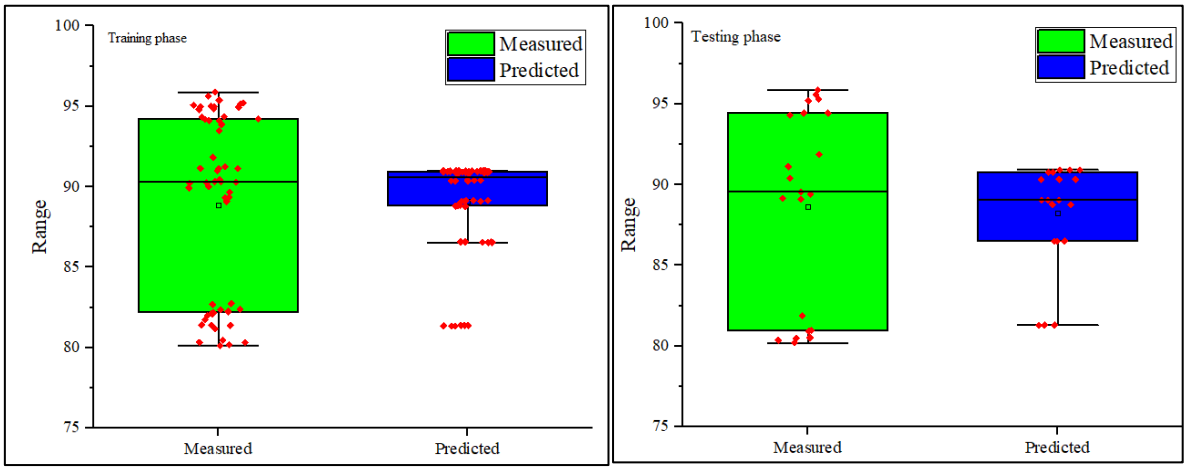

Figure 11- Boxplot comparison of measured and predicted η in training and testing phases.

3.Conclusions

This study demonstrated that combining pre-sedimentation with a multilayer horizontal roughing filter provides an effective and hydraulically robust treatment strategy for highly turbid surface waters (1500–2500 NTU). The lengths of the coarse gravel, medium gravel, and sand layers were selected based on engineering judgment and practical laboratory considerations to provide a hydraulically stable and representative configuration, with constant proportions maintained throughout the experiments to isolate the effects of total effective filter length. Accordingly, the present results should be interpreted as performance trends for the tested configurations rather than as identification of the optimal distribution of the individual media-layer lengths. Experimental results from 81 controlled runs showed that turbidity removal efficiency consistently exceeded 80 % under all tested conditions and reached values as high as 95–97 % at extended filter lengths. Among the investigated parameters, effective filter length was identified as the dominant design variable. Increasing the filter length from 260 cm to 450 cm resulted in an average improvement in turbidity removal efficiency of approximately 9–10 percentage points, regardless of filtration velocity. For example, at a filtration velocity of 0.20 m h^{-1}, mean efficiency increased from ≈ 85.3 % to 94.8 %, while similar gains (≈ 9.2–9.5 %) were observed at 0.60 and 1.00 m h^{-1}. Although filter length was found to be the dominant design parameter, the tested range was limited to the dimensions feasible in the laboratory model; therefore, the study does not claim determination of the absolute optimum filter length. Although the experimental results show that longer filter lengths improve turbidity removal within the tested range, the present study did not include a formal economic analysis. Therefore, the recommended configurations should be interpreted as hydraulically effective arrangements under laboratory conditions, not as economically optimal designs. A reliable techno-economic assessment would require site-specific data on construction cost, media cost, land availability, maintenance frequency, and scale-up effects, which were beyond the scope of this work. Future studies should integrate hydraulic performance with lifecycle cost analysis to identify the most feasible full-scale configuration.

Nevertheless, the final selection of filter length in practice should be based not only on turbidity removal efficiency but also on economic, spatial, and operational constraints, which were outside the scope of the present laboratory investigation. A full techno-economic assessment is therefore recommended in future field-scale studies to identify the most appropriate design length under local implementation conditions. In contrast, filtration velocity exerted a secondary influence, typically modifying efficiency within a narrower range of 3-5 % for a given filter length. Filtration time (10–30 min) showed minimal impact, with median efficiencies remaining nearly constant at ≈ 90 %, indicating that most particle removal occurs during the early stages of filtration. Sensitivity analysis using the Gamma Test confirmed a strong deterministic relationship between efficiency and the combined input parameters. The full-input configuration achieved a minimum Γ value of 0.0462 and a V-ratio of 0.1848, indicating high predictability and limited unexplained variance. This justified the development of a physically based saturation-type model, which was successfully calibrated using nonlinear least squares. The final model yielded physically meaningful parameters, including a maximum attainable efficiency of $\eta_{max} \approx 90.95$ %, a characteristic time scale of ≈ 3.8 min, and a very weak dependence on influent turbidity, confirming the robustness of the combined treatment system under extreme sediment loads. First and most importantly, all experiments in this study were conducted using a laboratory-scale physical model under controlled conditions. Although this approach ensured high experimental precision, the hydraulic behavior and sediment transport processes may differ in full-scale field systems. Therefore, the applicability of the proposed relationships should be further validated through pilot- or field-scale investigations. Despite the robust experimental dataset and modeling framework presented in this study, several limitations should be acknowledged. First and most importantly, all experiments were conducted using a laboratory-scale physical model under controlled conditions, and therefore the hydraulic behavior and operational performance may differ under full-scale field conditions. In addition, the experiments were performed using a single sediment source with specific particle-size characteristics; consequently, the observed removal efficiencies may vary for waters containing different sediment compositions, mineralogy, or particle-size distributions. The tested range of filter lengths was constrained by the laboratory setup, meaning that the results identify performance trends rather than the absolute optimal filter configuration. The distribution of media-layer thicknesses was kept constant to isolate the effect of total filter length, and alternative layer configurations were not investigated. Finally, the analysis focused primarily on turbidity removal performance, while long-term clogging behavior, economic considerations, and broader water quality parameters were beyond the scope of this investigation. Distributional analyses (histogram, boxplot, and violin plots) showed that while measured efficiencies exhibited multimodal variability, the model predictions formed a stable, unimodal distribution centered around 89–91%. This behavior reflects the model's role as a performance assessment and interpretive tool, rather than a pointwise empirical fit. In summary, the integrated experimental–modeling framework provides a low-cost, scalable, and physically interpretable approach for evaluating roughing filtration systems under high turbidity

conditions. The findings highlight that filter length is far more influential than operational adjustments such as filtration time, offering clear guidance for practical design and implementation in resource-limited regions.

Author Contributions

All authors contributed equally to the conceptualization of the article and writing of the original and subsequent drafts.

Data Availability Statement

The dataset is included in the paper.

Ethical Considerations

The authors avoided data fabrication, falsification, and plagiarism, and any form of misconduct.

Conflict of Interest

The authors declare no conflicts of interest.

3. References

Acharya, Y., Parajuli, A.P., 2026. Sustainable turbidity removal in urban water treatment using dual-layered crushed overburnt bricks and sand filters. International Journal of Energy and Water Resources, 10(3), p.87. https://doi.org/10.1007/s42108-026-00506-8

Aluah, D., Adongo, T.A., Shaibu, A.G., 2025. Performance Assessment of a Locally Constructed Wastewater Sludge Filter in the Tolon District of the Northern Region of Ghana. Ghana Journal of Science, Technology and Development, 11(1), pp.1-20. https://www.preprints.org/manuscript/202601.0868https://doi.org/10.47881/502.967x

Awandu, W., Wiesemann, J.U., Lehmann, B., 2025. Performance of horizontal roughing filter technology for safe drinking water access in rural developing economies. Water Science, 39(1), pp.388-398. https://doi.org/10.1080/23570008.2025.2574766

Babaei, F., Ehrampoush, M. H., Eslami, H., Ghaneian, M. T., Fallahzadeh, H., Talebi, P., Ebrahimi, A.A., 2019. Removal of linear alkylbenzene sulfonate and turbidity from greywater by a hybrid multi-layer slow sand filter microfiltration ultrafiltration system. Journal of Cleaner Production, 211, pp. 922-931. https://doi.org/10.1016/j.jclepro.2018.11.255

Bachar, N., Lindenstrauss, N., David, S., Mirkin, M., Polani, N., Gueta, O., Ronen, A., 2024. Improving Water Quality by Combined Sedimentation and Slow Sand Filtration: A Case Study in a Maasai Community, Tanzania. Applied Sciences, 14(20), p. 9467. https://doi.org/10.3390/app14209467

Duran Romero, D.A., de Almeida Silva, M.C., M. Chaúque, B. J., and D. Benetti, A., 2020. Biosand filter as a point-of-use water treatment technology: influence of turbidity on microorganism removal efficiency. Water, 12(8), p. 2302. https://doi.org/10.3390/w12082302

El-Taweel, G.E. and Ali, G.H., 2000. Evaluation of roughing and slow sand filters for water treatment. Water, air, and soil pollution, 120(1), pp. 21-28. https://doi.org/10.1023/A:1005252900175

Fereidonian Dashti, A., Abdul Aziz, H., Adlan, M.N. and Ibrahim, A.H., 2021. Effect of calcined limestone on the performance of roughing filter for turbidity removal of palm oil mill effluent. Journal of Hazardous, Toxic, and Radioactive Waste, 25(3), p. 04021013. https://doi.org/10.1061/(ASCE)HZ.2153-5515.000060

Fitriani, N., Wahyudianto, F. E., Salsabila, N. F., Mohamed, R. M. S. R., Kurniawan, S.B,. 2023. Performance of modified slow sand filter to reduce turbidity, total suspended solids, and iron in river water as water treatment in disaster areas. Journal of Ecological Engineering, 24(1). 10.12911/22998993/156009

Fouad, H.A., El-Hefny, R.M., Mohamed, M.A., 2016. Reuse of spent filter backwash water. Int. J. Civ. Eng. Technol, 7(4), pp.176-187.

Freitas, B. L. S., Terin, U. C., Fava, N. D. M. N., and Sabogal-Paz, L. P., 2021. Filter media depth and its effect on the efficiency of household slow sand filter in continuous flow. Journal of environmental management, 288, 112412. https://doi.org/10.1016/j.jenvman.2021.112412

García-Ávila, F. Zhindón-Arévalo, C. Álvarez-Ochoa, R. Donoso-Moscoso, S. Tonon-Ordoñez, M. D., Flores del Pino, L., 2020. Optimization of water use in a rapid filtration system: A case study. Water-Energy Nexus. 3, pp. 1-10

Hamzani, S., Syarifudin, A., Hati, F.I., Zubaidah, T., 2025. Combination Of Synthetic Filters With Ultrafiltration For The Treatment Of Cempaka River Water. JURNAL KESEHATAN LINGKUNGAN: Jurnal dan Aplikasi Teknik Kesehatan Lingkungan, 22(2), pp. 231-238. https://doi.org/10.31964/jkl.v22i2.990

He, W., Chen, X., Xu, C., Zhou, C., Wang, C., 2023. Internal interaction between chemically-pretreated polypropylene microplastics and floc growth during flocculation: Critical effect on floc properties and flocculation mechanisms. Separation and Purification Technology, 306, p. 122710. https://doi.org/10.1016/j.seppur.2022.122710

He, W., Luo, T., Chen, F., Sun, X., Yang, Z., 2025. Downflow and upflow sand filtration for removing turbid particles with diverse morphological and surface-charge characteristics: Comparisons of filtered water quality and head loss distribution. Separation and Purification Technology, 354, 128678. https://doi.org/10.1016/j.seppur.2024.128678

Jibhakate, M.L., Bhorkar, M.P., Bhole, A.G., Baitule, P.K., 2017. Reuse & recirculation of filter backwash water of water treatment water. Int. J. Eng. Res. Appl, 7(4), pp. 60-63.

Khan, Z., Farooqi, R., 2011. Roughing filtration as an effective pre-treatment system for high turbidity water. Water Science and Technology, 64(7), pp. 1419-1427.https://doi.org/10.2166/wst.2011.317

Kim, S., Eckart, K., Sabet, S., Chiu, P. C., Sapkota, A. R., Handy, E. T., Sharma, M., 2021. Escherichia coli reduction in water by zero-valent iron–sand filtration is based on water quality parameters. Water, 13(19), p. 2702. https://doi.org/10.3390/w13192702

Mao, H., Li, S., Lan, S., Guo, S., Huang, Y., Huang, Z., Li, X., 2021. Uniform flow field design in porous media filter tower and experimental verification. Process Safety and Environmental Protection, 150, pp. 68-78. https://doi.org/10.1016/j.psep.2021.03.053

Moreira, V.R., Guimarães, R.N., Moser, P.B., Santos, L.V., de Paula, E.C., Lebron, Y.A., Amaral, M.C., 2023. Restrictions in water treatment by conventional processes (coagulation, flocculation, and sand-filtration) following scenarios of dam failure. Journal of Water Process Engineering, 51, p. 103450. https://doi.org/10.1016/j.jwpe.2022.103450

Mtsweni, S., Bakare, B.F., Rathilal, S., 2025. Artificial Neural Network-Based Prediction of Clogging Duration to Support Backwashing Requirement in a Horizontal Roughing Filter: Enhancing Maintenance Efficiency. Water, 17(15), p. 2319. https://doi.org/10.3390/w17152319

Napotnik, J.A., Baker, D., Jellison, K.L., 2017. Effect of sand bed depth and medium age on Escherichia coli and turbidity removal in biosand filters. Environmental Science and Technology, 51(6), pp. 3402-3409. 10.1021/acs.est.6b05113.

Nieto, P.G., García-Gonzalo, E., Puig-Bargués, J., Solé-Torres, C., Duran-Ros, M., Arbat, G., 2020. A new predictive model for the outlet turbidity in micro-irrigation sand filters fed with effluents using Gaussian process regression. Computers and Electronics in Agriculture, 170, p. 105292. https://doi.org/10.1016/j.compag.2020.105292

Nouri, M., Nemati Varnosfaderany, M., Mirghaffari, N., Allafchian, A.R., 2025. Monitoring the state of wastewater treatment efficiency at stone cutting industry (Case study: Mahmoud Abad Industrial Town, Isfahan). Journal of New Approaches in Water Engineering and Environment, 4(1), pp. 145-163. https://doi.org/10.22034/nawee.2025.494536.1123

Onyutha, C., Okello, E., Atukwase, R., Nduhukiire, P., Ecodu, M., Kwiringira, J. N., 2024. Improving household water treatment: using zeolite to remove lead, fluoride and arsenic following optimized turbidity reduction in slow sand filtration. Sustainable Environment Research, 34(1), p. 4. https://doi.org/10.1186/s42834-024-00209-x

Shakeri yousefi, Sh. Najarchi, M., Fuladipanah, M., Rabani Bidgoli, M., 2025. Machine Learning models for High-Accuracy Prediction of Energy Dissipation Through Gabion Sills Downstream of Spillways. Journal of New Approaches in Water Engineering and Environment, 4(2), pp. 91-106. https://doi.org/10.22034/nawee.2025.507107.1140

Solgi, E., Beigmohammadi, F., Kiani, K., 2026. Investigating the Drinking Water Quality and Associated Human Health Risks in Sahneh City. Journal of New Approaches in Water Engineering and Environment, 5(5), pp. 110-127. https://doi.org/10.22034/nawee.2025.491922.1120

Tran, H.D.M., Kamada, K., Fujioka, T., 2024. Direct filtration of low-turbidity water by fixed-bed ion exchange treatment. Desalination and Water Treatment, 320, p. 100659. https://doi.org/10.1016/j.dwt.2024.100659

Verma, S., Daverey, A., Sharma, A., 2017. Slow sand filtration for water and wastewater treatment–a review. Environmental Technology Reviews, 6(1), pp. 47-58. https://doi.org/10.1080/21622515.2016.1278278

Xie, Z., Wang, S., Shen, Y., 2022. Particle-scale modelling of rapid granular filtration in a dual-media filter. Separation and Purification Technology, 302, p. 122076. https://doi.org/10.1016/j.seppur.2022.122076.

Zeng, J., Chen, S., Wan, K., Li, J., Hu, D., Zhang, S. Yu, X., 2020. Study of biological up-flow roughing filters designed for drinking water pretreatment in rural areas: using ceramic media as filter material. Environmental technology. https://doi.org/10.1080/09593330.2018.1530304